Effect of bias voltage on microstructure and optical properties of Al_2O_3 thin films prepared by twin targets reactive high power impulse magnetron sputtering

Guangxue Zhou[a], Langping Wang[a,*], Xiaofeng Wang[a], Yonghao Yu[b,*], Andreas Mutzke[c]

[a] State Key Laboratory of Advanced Welding and Joining, Harbin Institute of Technology, Harbin 150001, P.R. China

[b] Academy of Fundamental and Interdisciplinary Science, Harbin Institute of Technology, Harbin 150001, P.R. China

[c] Max-Planck-Institut für Plasmaphysik, Wendelsteinstrasse 1, D-17491 Greifswald, Germany

* Corresponding author
Professor Langping Wang
E-mail addresses: aplpwang@hit.edu.cn.
Tel: +86-451-86418728
Fax: +86-451-86416186

Dr. Yonghao Yu
E-mail addresses: yhyu@hit.edu.cn

Submitted to: ***VACUUM***

(With 8 figures)

ABSTRACT

Al_2O_3 thin films were deposited on silicon (100) and tin-doped indium oxide (ITO) substrates by twin targets reactive high power impulse magnetron sputtering (TTR-HiPIMS). Effects of the substrate bias voltage (V_b) on microstructure, surface morphology, chemical composition and optical transmittance of the deposited films were investigated by grazing incidence X-ray diffraction (GIXRD), atomic force microscopy (AFM), X-ray photoelectrons spectroscopy (XPS) and Ultra violet-visible-near infrared (UV-visible-NIR) spectra, respectively. The AFM scans showed that increasing the bias voltage (V_b) from 0 to -40 V caused the weakly crystalline film to evolve into fully crystalline Al_2O_3 film at temperatures as low as 230 ℃. However, when V_b reached -60 V, the crystallinity decreased. This result was also confirmed by GIXRD patterns, which showed that the best crystallinity of Al_2O_3 in γ phase was obtained for film deposited at a bias of -40 V. Besides, with the increase of V_b, the deposition rate decreased from 88 to 70 nm/h, and the O/Al ratio of the as-deposited films reduced from 1.53 to 1.44. The binary collision approximation (BCA) Monte-Carlo code SDTrimSP was also used to calculate the sputter yield of Al and Al_2O_3. It was found that the sputter yield of Al_2O_3 was about 1/8 of Al, which is supposed to be one of the main reasons for the observed low deposition rate. UV-vis-NIR transmittance spectra of Al_2O_3 films deposited under different bias voltages were evaluated after deposition on ITO substrates. The results revealed that all the as-deposited films had high optical transmittance ($\approx$ 80%) in the wavelength

range of 200-800 nm. Moreover, a marginal decrease of the transmittance was also observed with increasing V_b.

Keywords: Al_2O_3 film; twin targets sputtering; HiPIMS; Pulsed bias voltage; Optical properties; SDTrimSP;

1. INTRODUCTION

Aluminum oxide (Al_2O_3) thin films have been widely known for its high hardness, good chemical inertness, zero electrical conductivity and excellent optical transparency [1, 2]. Applications reported for these outstanding properties include wear and corrosion resistances, catalysis, microelectronics, diffusion and thermal barriers and optical protection [3-5]. There exist many different crystal structures of Al_2O_3: including α, γ, κ, θ, δ, η and χ, let alone the amorphous state [2]. Due to this polymorphism, the properties of the Al_2O_3 thin films are strongly influenced by the deposition technique, which determine the formation of a particular phase or phase mixtures [6, 7]. In recent years, there has been a considerable amount of work pertaining to deposit Al_2O_3 thin films by different methods, a typical list will involve, for instance, chemical vapor deposition [8], sol-gel method [9], filtered cathodic vacuum arc deposition [10], atomic layer deposition [11], E-beam evaporation [12], plasma spray [13], pulsed laser deposition [14] and sputter deposition [15-18]. Among these methods, sputter deposition and, more specifically, reactive high power impulse magnetron sputtering (R-HiPIMS) technique has been identified as superior to other techniques in terms of film density, phase tailoring and adhesion strength with substrate [15, 19]. However, for reactive magnetron sputtering, in general, the as-deposited Al_2O_3 films are often in amorphous state. To deposit a well-crystallized Al_2O_3 phases, elevated substrate temperatures (> 300 ℃) or post-deposition annealing are generally required [20]. Therefore, in many applications, there is a strong drive to

grow high quality crystalline Al_2O_3 films at much lower temperatures in order to minimize deposition cycling times and allow the use of thermally sensitive substrate materials [21, 22].

In addition to the microstructure, particular attention must be given to the target poisoning, and the consequent arcing problem with respect to reactive sputter deposition of insulating materials. The arc events often result in potential shifts, and therefore in non-defined process conditions. Moreover, micro-arcs will also cause layer imperfections in the film, which are particularly detrimental to the performance of optical or corrosion resistant films. It may also lead to damage of the magnetron sputtering power supply [23-25].

Within the deposition methods utilized, twin targets reactive high power impulse magnetron sputtering (TTR-HiPIMS) seems to offer the potential to solve the problems mentioned above [26]. Different from the traditional single target unipolar HIPIMS, in TTR-HiPIMS, each target acts alternatively as an anode and a cathode, and the power is supplied to the momentary cathode in pulses of high power density, while maintaining the time-averaged power in values similar to those during dc magnetron sputtering. This mode of operation results in generation of ultra-dense plasmas which is orders of magnitude higher than those achieved by conventional dc magnetron sputtering [19, 27]. Additionally, the closed field twin targets configuration not only offering the possibility of virtually arc-free deposition of insulating thin films, but also confine the plasma between the targets, increases the

efficiency of ionizing collisions, and thereby produces a high flux of ions at the substrate [28, 29]. Thus, the TTR-HiPIMS plasma offers the opportunity to increase adatom mobility of the condensing species and provides conditions that favor to deposit crystalline Al_2O_3 films at low temperature.

Our previous work showed that γ-Al_2O_3 thin films can be grown at relatively low substrate temperatures (300 ℃) [26]. To further lower the crystalline temperature of Al_2O_3 films, in the present study, a synchronized pulse bias was used to enhance the ion bombardment of the growing film. The effect of substrate bias voltage (V_b) on the microstructure, the chemical composition and optical properties of the as-deposited films have been investigated. Besides, for a better understanding of low deposition rate, theoretical calculation, by using binary collision approximation (BCA) program SDTrimSP, was also carried out to investigate the sputter yield of Al and Al_2O_3.

2. EXPERIMENTAL

Al_2O_3 thin films were deposited using a custom built vacuum chamber, as described in detail elsewhere [26]. The sputtering system is equipped with two unbalanced magnetrons with a directly water-cooled planar aluminum target (100 mm in diameter and 4 mm in thickness). The magnetrons were in a commonly used closed-field configuration. Silicon (100) wafers ($30 \times 30 \times 0.7$ mm^3) and tin-doped indium oxide (ITO) ($30 \times 30 \times 2$ mm^3) plates, cleaned consecutively in an ultrasonic bath with acetone and ethanol, were used as substrates. Prior to the deposition, the

targets were sputter cleaned in an argon atmosphere for 5 min with a shutter shielding the substrate. Moreover, silicon (100) and ITO substrates were heated up to approximate 230 ± 10 ℃. The base pressure in the vacuum chamber was kept lower than 1×10^{-3} Pa, then an ultrahigh purity gas mixture consisting of 50 sccm Ar and 14 sccm O_2 was admitted into the chamber to allow the targets operate in the poisoned mode. The total working pressure was maintained at 0.2 Pa by adjusting the throttle valve. The film thicknesses were fixed to about 150 nm.

The Al targets were powered with a bipolar pulsed AC power supply, and for all experiments regarding the deposition of the Al_2O_3 films, an average power of 360 W was applied to the two targets. Moreover, constant TTR-HiPIMS pulse parameters, pulse-on-time $t_{on} = 40$ μs, pulse-off-time between two consecutive pulse $t_{off} = 200$ μs and frequency f = 2000 Hz were used, which permits the targets operating effectively without severe arcing effects, as proven in our previous work [26]. For additional control of the deposition process, a synchronized pulse bias power supply, with a bias width of 30 μs and voltages of -20, -40 or -60 V in the negative periods, was connected to the substrate during deposition. The bias voltage, discharge voltage and current waveforms were recorded with two independent Tektronix TDS2014C oscilloscopes. In order to find the appropriate parameter combination to synthesize crystalline Al_2O_3 films, the bias voltage was varied as displayed in Table 1.

Table 1 Process parameters for Al_2O_3 thin films deposition

Process	TTR-HiPIMS	
Process parameters	Target material	Aluminum
	Target-substrate distance (mm)	100
	Substrate temperature (℃)	230
	Base pressure (Pa)	$< 1.0 \times 10^{-3}$
	Operating pressure (Pa)	0.2 Pa
	Ar flow rate (sccm)	50
	O_2 flow rate (sccm)	14
	Average power (W)	360
	Bias voltage (V)	0, -20, -40, -60

Fig. 1(a) shows typical discharge voltage and current waveforms of the TTR-HiPIMS pulses used for Al_2O_3 film depositions. Similarly, examples of the bias voltage waveforms used in this study are shown in Fig. 1(b). It can be seen that each TTR-HiPIMS period consisted of two single oscillations, which means that when one target is sputtered by positive ions, the other one is discharged by electrons or negative ions, and vice versa. The periodic polarity changing not only suppress arcing, but also effectively maintains ‘clean’ target surfaces, allowing long term stable deposition conditions [25]. Note that the voltage and current gradually increase to

their maximum value during the pulse-on-time, and then gradually decay, reaching zero before the end of the period.

The crystal structure of the as-deposited Al_2O_3 films were analyzed by X-ray diffraction (GIXRD; Empyrean, PANalytical), using Cu Kα radiation (40 kV and 40 mA) operated at an incidence angle of 1° (with the incident beam at θ = 1°). The elemental composition of the films was examined by X-ray photoelectron spectrometer (XPS; ESCALAB 250Xi, Thermo Fisher Scientific) by using Al Kα X-ray source (1486.6 eV). The film thickness on silicon substrates was determined by using a surface profilometer (DektakXT, Burker Corporation) along a step made through a shadow mask immediately after deposition. The deposition rate could be easily calculated from the film thickness and the deposition time. The surface morphology of the as-deposited films was studied using an atomic force microscope (AFM; Dimension Icon, Bruker) in tapping mode. In order to confirm the surfaces' uniformity, AFM scans over multiple random 1×1 μm^2 areas were performed for each sample. The optical transmittance of the films formed on ITO substrates were recorded by using ultra violet-visible-near infrared (UV-vis-NIR) double beam spectrophotometer (Lambda 950, PerkinElmer Corporation) in the wavelength range of 200 - 800 nm.

3. RESULTS AND DISCUSSION

3.1 Surface morphology and microstructure

The AFM technique was used to obtain the morphology information of the as-deposited films. Fig. 2 shows typical 1 $\times$ 1 μm^2 3D AFM topographic images of the films deposited on silicon substrates at a substrate bias of 0, -20, -40 and -60 V. In the case of film grown with a grounded substrate, small grains were visible indicating that a few amount of nanocrystallized Al_2O_3 could already be present in the film, as also revealed by its low root-mean-square (rms) surface roughness value of 1.9 nm. This suggests that relatively low temperature (230 ℃) alone cannot supply enough energy to the near-surface atoms of the growing film and thus cannot form poly-crystalline Al_2O_3 film. For the films deposited at a bias voltage of -20 and -40 V, the surfaces were dense and uniform. As a consequence, the rms roughness values were found to be 2.25 and 2.14 nm, respectively. The increase in atomic mobility with increasing bias magnitude created more nucleation sites and enables thermodynamically favored grains to grow, thereby resulting in better crystalline films [30]. However, at higher bias voltage (-60 V), the film surface became slightly rougher with closely spaced pits features. Accordingly, the roughness value was increased to 3.37 nm. The features resulted from the excessive ion bombardment [31]. In addition, for the film deposited with a bias voltage of -20, -40 and -60 V, the reduced grain size observed is a result of increased ions' (Ar^+, Al^+, $AlOH^+$, O_2^+) bombardment [32, 33].

GIXRD analysis, obtained on films deposited on Si (100) substrates was done to ascertain the changes in the structure of the as-deposited films as a function of bias

voltage. Fig. 3 presents the GIXRD patterns for films deposited with substrate bias voltages of 0, -20, -40 and -60 V. The vertical lines correspond to the standard diffraction peaks of γ-Al_2O_3 (JCPDS 10-0425). According to these results, the film deposited at grounded substrate exhibited weak peaks at 45.18 ° and 66.47 °, which correspond to the (4 0 0) and (4 4 0) directions of γ-Al_2O_3. As the bias voltage was increased to -20 and -40 V, an additional γ-Al_2O_3 peak at about 37 ° and a distinct increase of the peak intensity were observed, indicating an improved crystal quality of the Al_2O_3 films. This is primarily due to the positive ion' (Ar^+, Al^+, $AlOH^+$, O_2^+) bombardment with the help of the substrate bias which supplies an additional kinetic energy to the surface and near-surface region of the growing films, compensating for the insufficient energy provided by the heating temperature. In addition, energy supplied from energetic negative ions (O_2^-, OH^- and O^-), which has proved to be essential in the reactive case [34, 35] , may also responsible for the observed low-temperature γ-Al_2O_3 growth [36, 37]. The ion bombardment during the deposition process removes also the loosely bound atoms at the surface and leads to a higher activation of the condensing particles, which is in favor for the formation of poly-crystalline Al_2O_3 [15, 38]. However, when the film was deposited at the bias voltage of -60 V, a remarkable reduction in the peak intensity can be observed. This is because the momentarily temperature increase of the film caused by the ion bombardment cannot efficiently anneal the defects caused by the bombardment flux. This trend is consistent with the AFM results as well as previous reports on

crystallographic changes [31, 39]. Therefore, the optimum bias magnitude for the deposition of crystalline Al_2O_3 film in this study is -40 V.

The presence of energetic ion and neutral bombardment during the deposition process can also leads to the XRD peaks shifting towards higher angles for tensile stress and towards lower angles for compressive stress [30]. Analyzing the presented diffraction diagrams in Fig. 3, it can be seen that the peaks were all slightly left-shifted, and the deviation became larger with the increasing V_b. Two deposition regimes may account for this compressive stress generation. On the one hand, the compressive stress exhibited in Al_2O_3 films synthesized at 0.2 Pa could be derived from the atomic peening effect [40, 41]. In such a scenario, the argon, oxygen and sputtered particles have long mean free path (≈ 50 mm in 0.2Pa) and high momentum with fewer collisions, thus bringing about a compressive stress in the film. On the other hand, for the same TTR-HiPIMS operating parameters, the presence of bias voltage led to an additional ion bombardment effect, and hence introduced a larger residual compressive stress with the increase of V_b [42].

3.2 Deposition rate and elemental composition

3.2.1 Experimental results

The deposition rate of the films grown at various bias voltages was calculated and showed in Fig. 4. As can be seen that the deposition rate decreased almost linearly from 88 to 70 nm/h while the bias voltage was increased from 0 to -60 V. The physical

reasons for this apparently low deposition rate can be explained as follows: (i) Self-sputtering and process gas recycling: As one version of HiPIMS, the most important and widely recognized reason for the significantly low deposition rate are self-sputtering (ions of the sputtered vapor that are attracted back to the target and participate in the sputtering process) and process gas recycling (gas atoms coming from the target that are subsequently ionized, and then drawn back to the target again) [43-46]. (ii) Low sputter yield caused by the target poisoning. As noted above, the discharge was operated at the fully poisoned mode, whose sputter yield is significantly lower than that of pure Al, as also will be explained in the simulation section. (iii) Low working pressure. The low working gas pressure used in this study (0.2 Pa), while ensured high energies and high surface mobility for the bombarding particles (both sputtered and backscattered) due to the low probability of gas phase collisions, it also reduced the number of ions that strike the target, and thus led to a low deposition rate [47]. (iv) Sideway deposition. It was previously shown that the presence of a dual magnetron configuration will result in an ions drift outwards in the vicinity of the cathode (parallel to the substrate surface), hence leading to a decreased deposition efficiency at the substrate position (perpendicular to the drift direction) [48]. (v) Collisional impact of energetic particles. In a TTR-HiPIMS process, all the energetic species, such as neutral particles, ions, and other radicals, contributed to the energy impact to the growing film through collisions and promoted densification and subsequent re-sputtering of the films. Therefore, another possible reason why the

as-deposited Al_2O_3 films have the relatively lower growth rate may be their high density and strong re-sputtering effect [30, 35, 49].

To investigate the chemical composition and determine the surface oxidation states of films deposited with different substrate bias voltages, high resolution scans of Al 2p and O 1s energy regions for the films deposited on Si substrate are shown in Fig. 5 and 6, respectively. The binding energies were referenced with contaminated carbon peak in the films (Binding Energy = 284.6 eV) [50]. As can be seen from Fig. 5, the Al 2p spectra at 74.5 ±0.2 eV can be well fitted into one intense peak, indicated that the aluminum presented in the film was bound as Al^{3+}. Also, no peak pertaining to metallic Al (Binding Energy = 71.3 eV) was observed, showing that the aluminum presented in the film was in the form of Al_2O_3 [51]. The high resolution O1s scans of films deposited with different bias voltages are compared in Fig. 6. In all the cases studied, the O1s spectra shows a single, broad peak at 531.2 ±0.2 eV, indicating that the oxidic oxygen was the major species in the Al_2O_3 films rather than the absorption one, which locates at a higher binding energy [50, 52].

Varying the substrate bias potential does not only affect ion energy to the substrate, it may also have an influence on the chemical composition of the films [31, 53]. For the depositions reported here, quantitative analysis was carried out to study the influence of the bias voltage on the atomic O/Al ratios of the as-deposited films. Fig. 7 compares the experimental O/Al atomic ratios for all films. The film deposited without a substrate bias was found to be oxygen rich with an atomic O/Al ratio of 1.53.

As for films deposited at bias voltages of -20, -40 and -60 V, the elemental composition showed a gradual decrease in O/Al ratios from 1.51 to 1.44, which is in good agreement with earlier reports on different thin films [30]. This variation can be attributed to the well-known preferential sputtering effect. As we know, the substrate bias voltage relates directly to the ion energy, so increasing V_b leads to the enhancement of the momentum transfer to the atoms on the film surface, which means a larger re-sputtering effect for light atoms [30, 54, 55].

3.2.2 SDTrimSP simulations

For a better understanding of low deposition rate, theoretical calculation, by using binary collision approximation (BCA) program SDTrimSP, was also carried out to investigate the sputter yield difference between Al and Al_2O_3. SDTrimSP (SD = static-dynamic; SP = sequential and parallel processing), similar to the well-known program TRIM, but use the Krypton-Carbon interaction potential instead of Ziegler-Biersack-Littmark (ZBL) interatomic potential, which makes it more suitable to describe low energy collisions. Furthermore, SDTrimSP does not have the drawbacks that existed in TRIM, such as overestimates the yield for targets containing low atomic number (Z) elements with $Z < 14$ and underestimates it for heavy ones ($Z > 14$). SDTrimSP also contains a 1D, layered dynamic composition model that takes into account preferential sputtering as well as stoichiometry changes of each layer as a result of projectile ions incorporation and atomic mixing [55, 56].

Calculating the sputter yield of Al_2O_3 is more complex than pure Al because Al_2O_3 is a compound, so dynamic mode was used in this work to include the dynamical effects of the projectiles on the sputter yield. The surface binding energies for Al_2O_3 were calculated by averaging the elemental surface binding energies provided by SDTrimSP, controlled with the parameter isbv = 5 in the "tri.inp" input file. For a 380 eV normal incidence, the sputter yields of Al due to Ar^+ bombardment of pure Al and Al_2O_3 targets were 0.73 and 0.09, respectively. The main reasons for this large difference in sputter yield derived from the different masses as well as the differences in displacement and surface binding energies. In addition, O^+ impingements also contributed to the sputtering process. According to the SDTrimSP simulation, the Al sputter yield due to O^+ bombardment of Al_2O_3 was 0.12, which is larger than the one of Ar^+. However, considering the low O_2 partial pressure, this sputter yield difference will not have a significant effect on the combined deposition rate of Al_2O_3. Therefore, these factors explain the substantial drop of the deposition rate, as low as 1/8 of Al deposition rate in pure Ar.

3.3 Optical transmittance

Fig. 8 shows the optical transmission spectra of the films prepared onto ITO at different substrate bias. The transmittance of an uncoated ITO is shown for comparison. The results revealed that all the as-deposited films had high optical transmittance (≈ 80%) in the wavelength range of 200-800 nm. In addition, it is

clearly observed that the transmittance of the as-deposited films was slightly decreased with the increase of V_b. For the film deposited at $V_b \leq -40$ V, the decrease in optical transmission should be derive from the improvement in the crystallinity, as confirmed with GIXRD analysis results [57]. However, as for the film deposited at a bias of -60 V, combined with the effect of bias voltage on surface morphology, we can see that the increase in scattering centers due to excessive ion bombardment might be responsible for increased optical scattering, and consequently decreased transmittance [58].

4. CONCLUSIONS

Al_2O_3 thin films were deposited on Si (100) and ITO substrates by TTR-HiPIMS technique at temperatures as low as 230 ℃. Increasing the bias voltage (V_b) from 0 to -40 V caused the weakly crystalline film to evolve into fully crystalline γ-Al_2O_3 film. However, the crystallization got weaker with further increasing V_b. Besides, as V_b was increased from 0 to -60 V, the deposition rate decreased from 88 to 77 nm/h and so do the O/Al ratios of the as-deposited films. The calculated results showed that the sputter yield of Al_2O_3 was about 1/8 of pure Al, which is supposed to be one of the main reasons for the observed low deposition rate. The UV-vis-NIR spectroscopy analysis revealed that all the as-deposited films had high optical transmittance (≈ 80%) in the wavelength range of 200-800 nm. In addition, it is clearly observed that the transmittance of the as-deposited films was slightly decreased with the increase of V_b.

These results contribute towards understanding of the evolution of film composition and microstructure, and are illustrating a pathway for γ-Al_2O_3 growth at low substrate temperature. This may be technologically important for the deposition on heat sensitive substrate materials.

ACKNOWLEDGMENT

This work was financially supported by the fund of National Key Research and Development Program of China (2017YFC0111002).

REFERENCES

[1] M. Aguilar-Frutis, M. Garcia, C. Falcony, Optical and electrical properties of aluminum oxide films deposited by spray pyrolysis, Appl. Phys. Lett. 72 (1998) 1700-1702.

[2] W. Engelhart, W. Dreher, O. Eibl, V. Schier, Deposition of alumina thin film by dual magnetron sputtering: Is it γ-Al2O3?, Acta Mater. 59 (2011) 7757-7767.

[3] M. Shimada, T. Amazawa, T. Ono, S. Matsuo, H. Oikawa, Ultrathin Al2O3 and AlN films deposited by reactive sputter using advanced electron cyclotron resonance plasma source, Vacuum 59 (2000) 727-734.

[4] B. Segda, M. Jacquet, J. Besse, Elaboration, characterization and dielectric properties study of amorphous alumina thin films deposited by rf magnetron sputtering, Vacuum 62 (2001) 27-38.

[5] J.L. Wang, Y.H. Yu, S.C. Lee, Y.W. Chung, Tribological and optical properties of crystalline and amorphous alumina thin films grown by low-temperature reactive magnetron sputter-deposition, Surf. Coat. Technol. 146 (2001) 189-194.

[6] E.B.W.H. Gitzen, Alumina as a ceramic material, 1970.

[7] X. Zhang, J. Zhu, L. Zhang, J. Han, S. Du, Low-temperature crystallization and hardness enhancement of alumina films using the resputtering technique, J. Non-Cryst. Solids. 362 (2013) 34-39.

[8] W. Koh, S.-J. Ku, Y. Kim, Chemical vapor deposition of Al2O3 films using highly volatile single sources, Thin Solid Films 304 (1997) 222-224.

[9] P. Yang, M. Yao, R. Xiao, J. Chen, X. Yao, Preparation of Al2O3 film by sol–gel method on thermally evaporated Al film, Vacuum 107 (2014) 112-115.

[10] Z.W. Zhao, B.K. Tay, D. Sheeja, Structural characteristics and mechanical properties of aluminium

oxide thin films prepared by off-plane filtered cathodic vacuum arc system, Surf. Coat. Technol. 167 (2003) 234-239.
[11] P. Boryło, K. Lukaszkowicz, M. Szindler, J. Kubacki, K. Balin, M. Basiaga, J. Szewczenko, Structure and properties of Al2O3 thin films deposited by ALD process, Vacuum 131 (2016) 319-326.
[12] N. Maiti, A. Biswas, R.B. Tokas, D. Bhattacharyya, S.N. Jha, U.P. Deshpande, U.D. Barve, M.S. Bhatia, A.K. Das, Effects of oxygen flow rate on microstructure and optical properties of aluminum oxide films deposited by electron beam evaporation technique, Vacuum 85 (2010) 214-220.
[13] R. Krishnan, S. Dash, R. Kesavamoorthy, C. Babu Rao, A.K. Tyagi, B. Raj, Laser surface modification and characterization of air plasma sprayed alumina coatings, Surf. Coat. Technol. 200 (2006) 2791-2799.
[14] G. Balakrishnan, S. Tripura Sundari, R. Ramaseshan, R. Thirumurugesan, E. Mohandas, D. Sastikumar, P. Kuppusami, T.G. Kim, J.I. Song, Effect of substrate temperature on microstructure and optical properties of nanocrystalline alumina thin films, Ceram. Int. 39 (2013) 9017-9023.
[15] W.D. Sproul, The reactive sputter deposition of aluminum Oxide coatings Using High Power Pulsed Magnetron Sputtering (HPPMS), 47th Annu. Tech. Conf. P. Soc. Vac. Coat. Dallas, Texas, April, 24-29, 2004, (2004).
[16] Y. Chiba, Y. Abe, M. Kawamura, K. Sasaki, Formation process of Al2O3 thin film by reactive sputtering, Vacuum 83 (2008) 483-485.
[17] J. Kohout, E. Bousser, T. Schmitt, R. Vernhes, O. Zabeida, J. Klemberg-Sapieha, L. Martinu, Stable reactive deposition of amorphous Al2O3 films with low residual stress and enhanced toughness using pulsed dc magnetron sputtering with very low duty cycle, Vacuum 124 (2016) 96-100.
[18] J.C. Ding, T.F. Zhang, R.S. Mane, K.-H. Kim, M.C. Kang, C.W. Zou, Q.M. Wang, Low-temperature deposition of nanocrystalline Al 2 O 3 films by ion source-assisted magnetron sputtering, Vacuum 149 (2018) 284-290.
[19] J.T. Gudmundsson, N. Brenning, D. Lundin, U. Helmersson, High power impulse magnetron sputtering discharge, J. Vac. Sci. Technol. A 30 (2012) 030801.
[20] M. Sridharan, M. Sillassen, J. Bøttiger, J. Chevallier, H. Birkedal, Pulsed DC magnetron sputtered Al2O3 films and their hardness, Surf. Coat. Technol. 202 (2007) 920-924.
[21] O. Zywitzki, G. Hoetzsch, Influence of coating parameters on the structure and properties of Al2O3 layers reactively deposited by means of pulsed magnetron sputtering, Surf. Coat. Technol. 86-87 (1996) 640-647.
[22] J. Wang, Y.-H. Yu, S.C. Lee, Y.-W. Chung, Tribological and optical properties of crystalline and amorphous alumina thin films grown by low-temperature reactive magnetron sputter-deposition, Surf. Coat. Technol. 146-147 (2001) 189-194.
[23] V. Kirchhoff, T. Kopte, T. Winkler, M. Schulze, P. Wiedemuth, Dual magnetron sputtering (DMS) system with sine-wave power supply for large-area coating, Surf. Coat. Technol. 98 (1998) 828-833.
[24] P.J. Kelly, R.D. Arnell, Control of the structure and properties of aluminum oxide coatings deposited by pulsed magnetron sputtering, J. Vac. Sci. Technol. A 17 (1999) 945-953.
[25] J. O'Brien, P.J. Kelly, Characterisation studies of the pulsed dual cathode magnetron sputtering process for oxide films, Surf. Coat. Technol. 142-144 (2001) 621-627.
[26] G. Zhou, L. Wang, X. Wang, Y. Yu, Deposition of nanostructured crystalline alumina thin film by twin targets reactive high power impulse magnetron sputtering, Appl. Surf. Sci. 455 (2018) 310-317.

[27] U. Helmersson, M. Lattemann, J. Bohlmark, A.P. Ehiasarian, J.T. Gudmundsson, Ionized physical vapor deposition (IPVD): A review of technology and applications, Thin Solid Films 513 (2006) 1-24.
[28] J. Musil, P. Baroch, Discharge in dual magnetron sputtering system, IEEE T. Plasma. Sci. 33 (2005) 338-339.
[29] M. Yusupov, E. Bultinck, D. Depla, A. Bogaerts, Behavior of electrons in a dual-magnetron sputter deposition system: a Monte Carlo model, New J. Phys. 13 (2011) 033018.
[30] X. Tang, F. Luo, F. Ou, W. Zhou, D. Zhu, Z. Huang, Effects of negative substrate bias voltage on the structure and properties of aluminum oxide films prepared by DC reactive magnetron sputtering, Appl. Surf. Sci. 259 (2012) 448-453.
[31] J. Rosén, S. Mráz, U. Kreissig, D. Music, J.M. Schneider, Effect of Ion Energy on Structure and Composition of Cathodic Arc Deposited Alumina Thin Films, Plasma Chem. Plasma P. 25 (2005) 303-317.
[32] T. Lin, L. Wang, X. Wang, Y. Zhang, Y. Yu, Influence of bias voltage on microstructure and phase transition properties of VO 2 thin film synthesized by HiPIMS, Surf. Coat. Technol. 305 (2016) 110-115.
[33] L. Bait, L. Azzouz, N. Madaoui, N. Saoula, Influence of substrate bias voltage on the properties of TiO 2 deposited by radio-frequency magnetron sputtering on 304L for biomaterials applications, Appl. Surf. Sci. 395 (2017) 72-77.
[34] J. Rosén, E. Widenkvist, K. Larsson, U. Kreissig, S. Mráz, C. Martinez, D. Music, J.M. Schneider, Reducing the impurity incorporation from residual gas by ion bombardment during high vacuum magnetron sputtering, Appl. Phys. Lett. 88 (2006) 191905.
[35] E. Wallin, J.M. Andersson, M. Lattemann, U. Helmersson, Influence of residual water on magnetron sputter deposited crystalline Al2O3 thin films, Thin Solid Films 516 (2008) 3877-3883.
[36] J.M. Andersson, E. Wallin, U. Helmersson, U. Kreissig, E.P. Münger, Phase control of Al2O3 thin films grown at low temperatures, Thin Solid Films 513 (2006) 57-59.
[37] J.M. Andersson, E. Wallin, E.P. Münger, U. Helmersson, Energy distributions of positive and negative ions during magnetron sputtering of an Al target in Ar/O[sub 2] mixtures, J. Appl. Phys. 100 (2006) 033305.
[38] M.M.S. Villamayor, J. Keraudy, T. Shimizu, R.P.B. Viloan, R. Boyd, D. Lundin, J.E. Greene, I. Petrov, U. Helmersson, Low temperature (Ts/Tm < 0.1) epitaxial growth of HfN/MgO(001) via reactive HiPIMS with metal-ion synchronized substrate bias, J. Vac. Sci. Technol. A 36 (2018) 061511.
[39] H. Hajihoseini, M. Kateb, S. Ingvarsson, J.T. Gudmundsson, Effect of substrate bias on properties of HiPIMS deposited vanadium nitride films, Thin Solid Films 663 (2018) 126-130.
[40] J.A. Thornton, D.W. Hoffman, Internal stresses in titanium, nickel, molybdenum, and tantalum films deposited by cylindrical magnetron sputtering, J. Vac. Sci. Technol. 14 (1977) 164-168.
[41] D.W. Hoffman, J.A. Thornton, Internal stresses in Cr, Mo, Ta, and Pt films deposited by sputtering from a planar magnetron source, J. Vac. Sci. Technol. 20 (1982) 355-358.
[42] I.-L. Velicu, V. Tiron, C. Porosnicu, I. Burducea, N. Lupu, G. Stoian, G. Popa, D. Munteanu, Enhanced properties of tungsten thin films deposited with a novel HiPIMS approach, Appl. Surf. Sci. 424 (2017) 397-406.
[43] D.J. Christie, Target material pathways model for high power pulsed magnetron sputtering, J. Vac. Sci. Technol. A 23 (2005) 330-335.
[44] A. Anders, Deposition rates of high power impulse magnetron sputtering: Physics and economics, J.

Vac. Sci. Technol. A 28 (2010) 783-790.
[45] J.T. Gudmundsson, D. Lundin, N. Brenning, M.A. Raadu, C. Huo, T.M. Minea, An ionization region model of the reactive Ar/O2high power impulse magnetron sputtering discharge, Plasma Sources Sci. T. 25 (2016) 065004.
[46] N. Brenning, J.T. Gudmundsson, M.A. Raadu, T.J. Petty, T. Minea, D. Lundin, A unified treatment of self-sputtering, process gas recycling, and runaway for high power impulse sputtering magnetrons, Plasma Sources Sci. T. 26 (2017) 125003.
[47] B.J.H. Stadler, Chapter 7 - Vapor Processes, in: L.F. Francis (Ed.) Materials Processing, Academic Press, Boston, 2016, pp. 513-588.
[48] M. Yusupov, E. Bultinck, D. Depla, A. Bogaerts, Elucidating the asymmetric behavior of the discharge in a dual magnetron sputter deposition system, Appl. Phys. Lett. 98 (2011) 131502.
[49] J. Emmerlich, S. Mráz, R. Snyders, K. Jiang, J.M. Schneider, The physical reason for the apparently low deposition rate during high-power pulsed magnetron sputtering, Vacuum 82 (2008) 867-870.
[50] N. Reddy, P. Bera, V.R. Reddy, N. Sridhara, A. Dey, C. Anandan, A.K. Sharma, XPS study of sputtered alumina thin films, Ceram. Int. 40 (2014) 11099-11107.
[51] X. Zhang, J. Zhu, L. Zhang, K. Kishimoto, S. Du, X. Yin, Crystallization of alumina films deposited by reactive magnetron sputtering with resputtering technique at low temperature, Surf. Coat. Technol. 228 (2013) S393-S396.
[52] S. Prasanna, G. Krishnendu, S. Shalini, P. Biji, G. Mohan Rao, S. Jayakumar, R. Balasundaraprabhu, Composition, structure and electrical properties of DC reactive magnetron sputtered Al2O3 thin films, Mat. Sci. Semicon. Proc. 16 (2013) 705-711.
[53] T. Kubart, R.M. Schmidt, M. Austgen, T. Nyberg, A. Pflug, M. Siemers, M. Wuttig, S. Berg, Modelling of sputtering yield amplification in serial reactive magnetron co-sputtering, Surf. Coat. Technol. 206 (2012) 5055-5059.
[54] N. Li, J.P. Allain, D.N. Ruzic, Enhancement of aluminum oxide physical vapor deposition with a secondary plasma, Surf. Coat. Technol. 149 (2002) 161-170.
[55] H. Hofsäss, K. Zhang, A. Mutzke, Simulation of ion beam sputtering with SDTrimSP, TRIDYN and SRIM, Appl. Surf. Sci. 310 (2014) 134-141.
[56] V.I. Shulga, Note on the artefacts in SRIM simulation of sputtering, Appl. Surf. Sci. 439 (2018) 456-461.
[57] Z.W. Zhao, B.K. Tay, G.Q. Yu, D.H.C. Chua, S.P. Lau, L.K. Cheah, Optical properties of aluminium oxide thin films prepared at room temperature by off-plane filtered cathodic vacuum arc system, Thin Solid Films 447-448 (2004) 14-19.
[58] Y. Hu, X. Diao, C. Wang, W. Hao, T. Wang, Effects of heat treatment on properties of ITO films prepared by rf magnetron sputtering, Vacuum 75 (2004) 183-188.

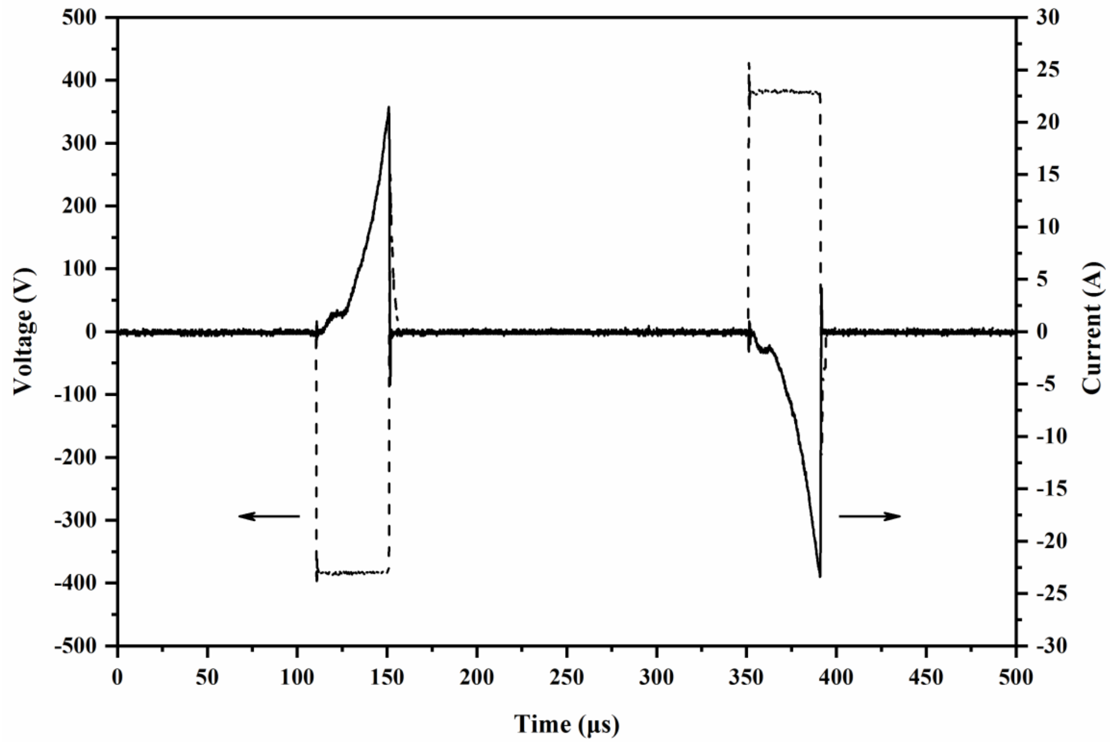

Voltage (V)
Current (A)
Time (µs)
500
400
300
200
100
0
-100
-200
-300
-400
-500
30
25
20
15
10
5
0
-5
-10
-15
-20
-25
-30
0
50
100
150
200
250
300
350
400
450
500

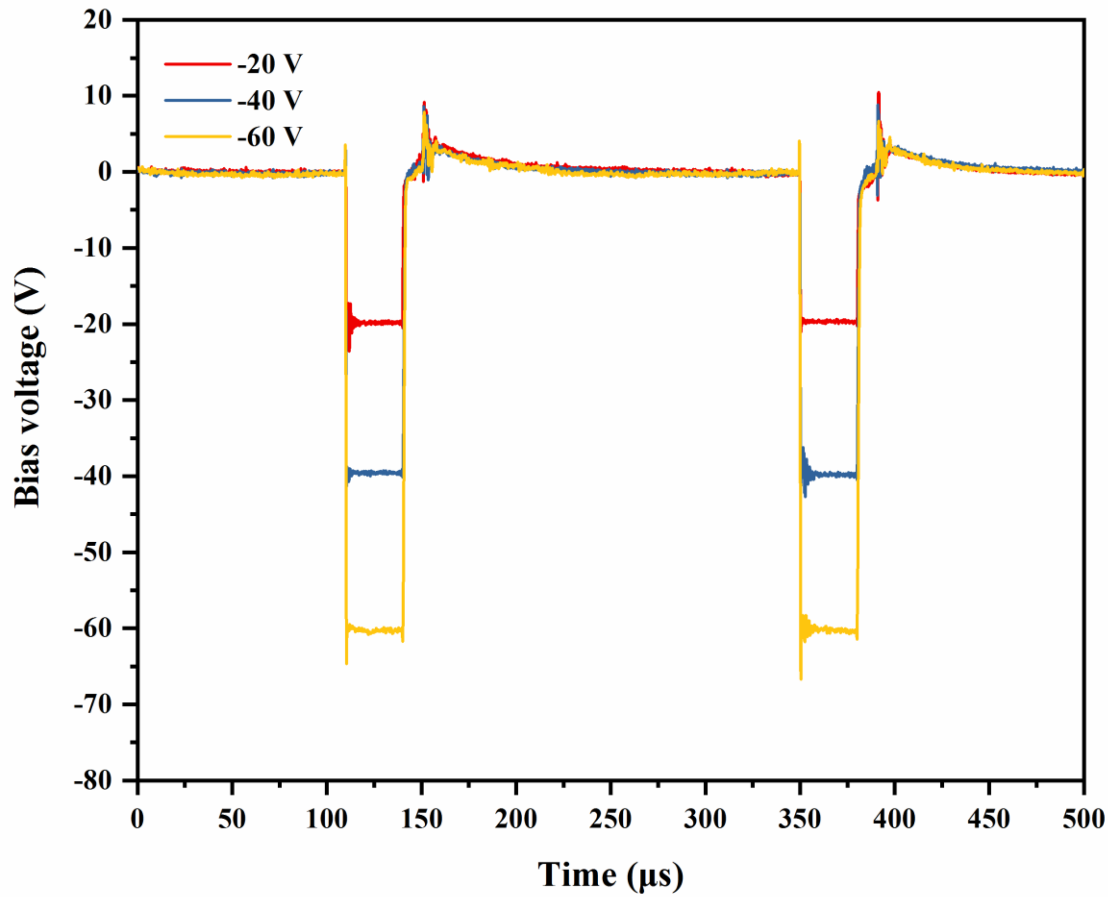

Fig. 1 (a) Typical discharge voltage (dashed) and current (solid) waveform in one TTR-HiPIMS period, (b) Bias voltage waveforms used for Al_2O_3 thin film depositions

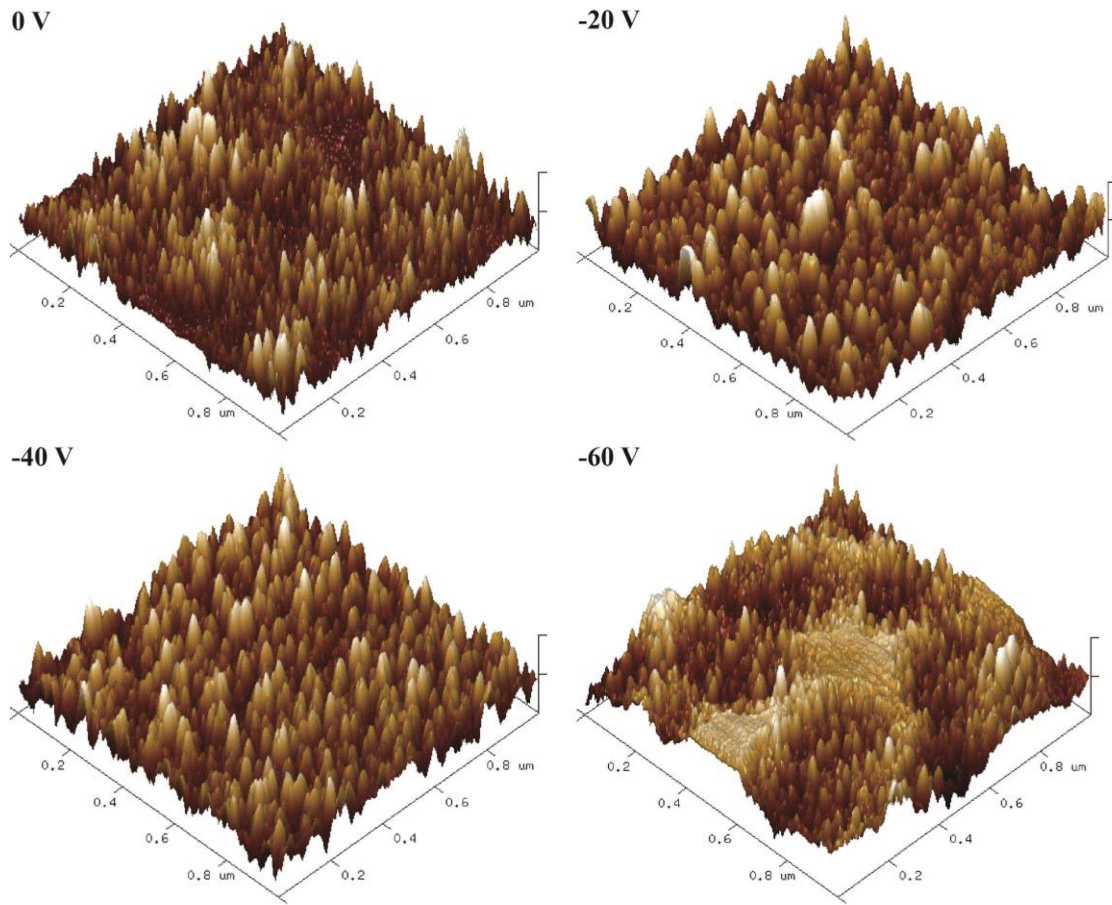

Fig. 2. AFM images of Al_2O_3 thin films deposited on Si (100) substrate at various bias voltages.

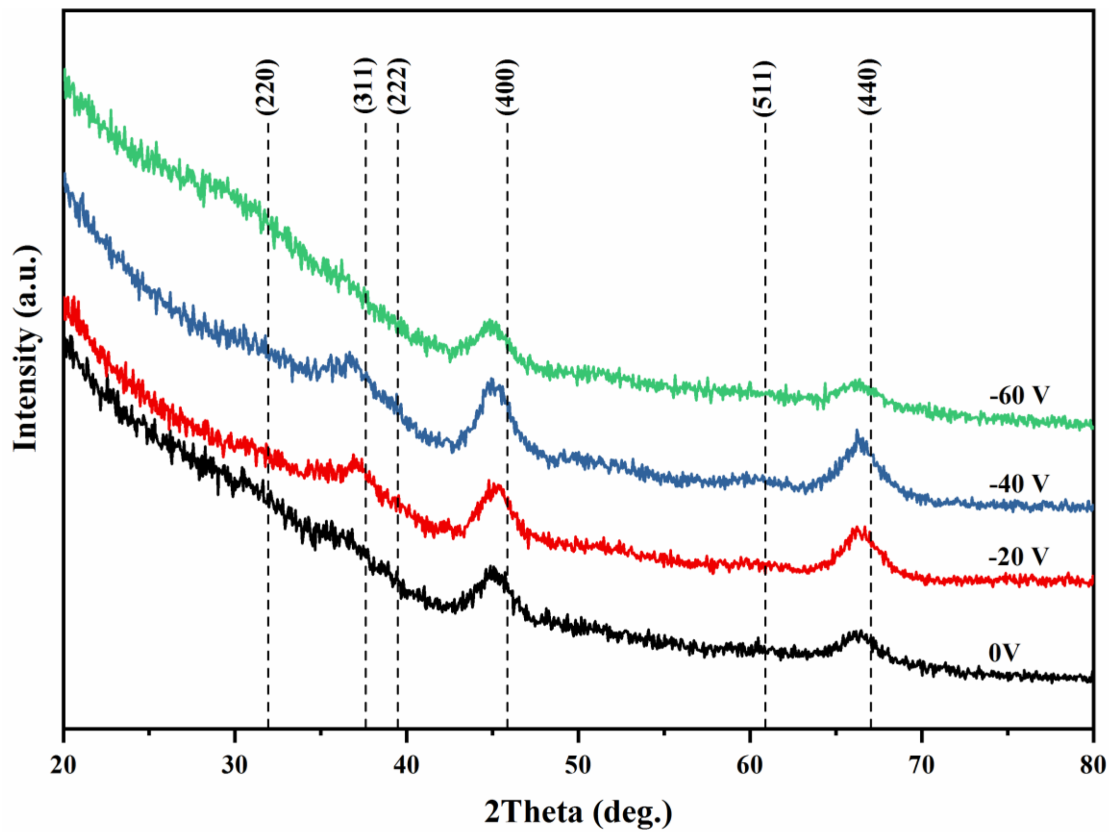

Fig. 3. GIXRD patterns of Al_2O_3 thin films deposited on Si (100) substrate at various bias voltages. The dash lines correspond to the standard diffraction peak positions of γ-Al_2O_3 (JCPDS 10-0425).

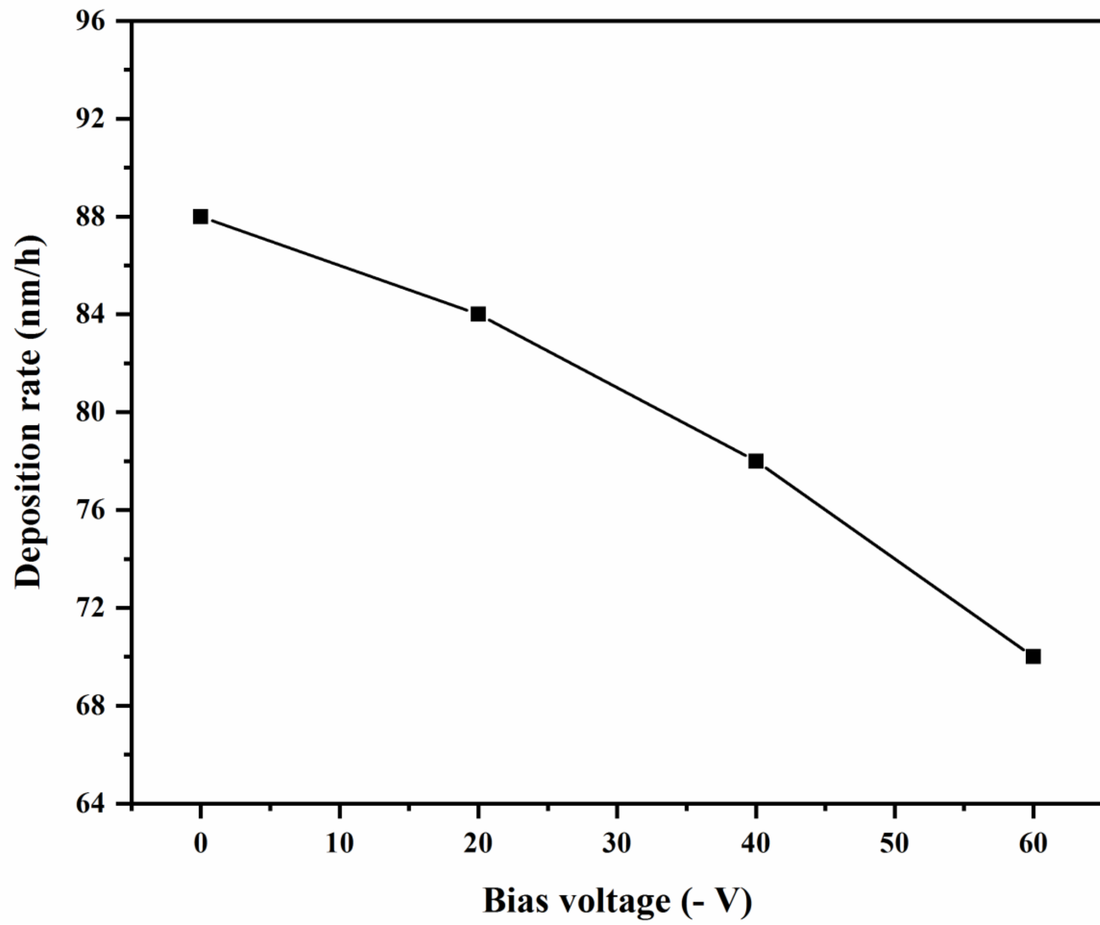

Fig. 4. Deposition rate of Al_2O_3 thin films as a function of bias voltage.

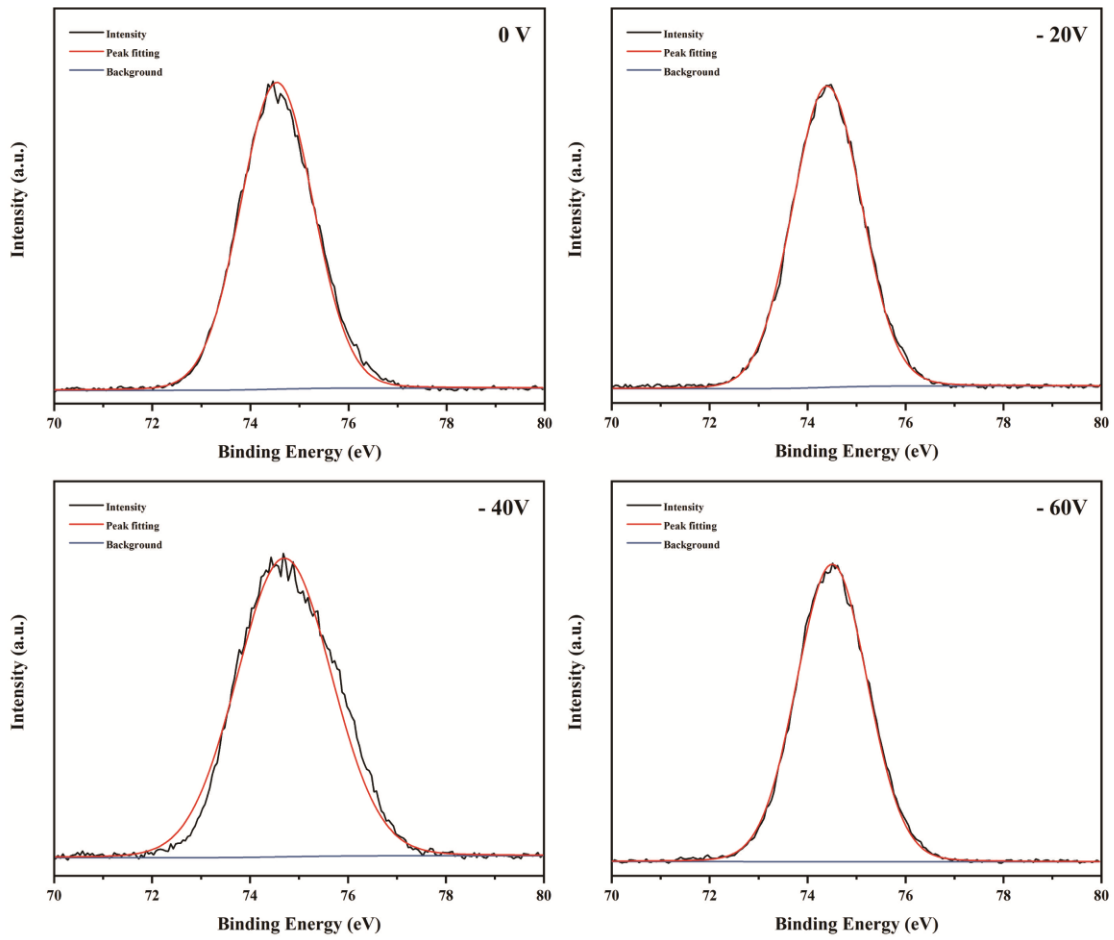

Fig. 5. Typical fitted curves of Al 2p XPS spectra of Al_2O_3 thin films deposited on Si (100) substrate at various bias voltages.

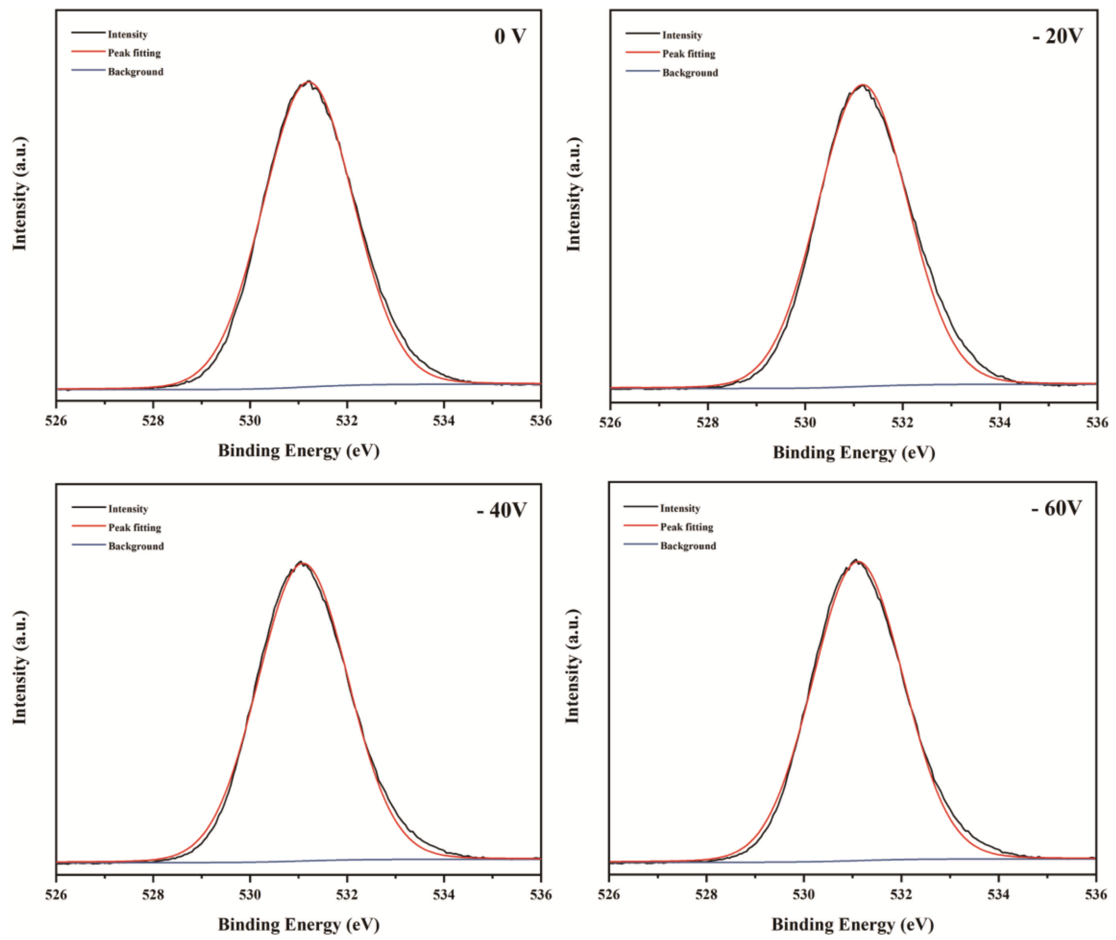

Fig. 6. Typical fitted curves of O 1s XPS spectra of Al_2O_3 thin films deposited on Si (100) substrate at various bias voltages.

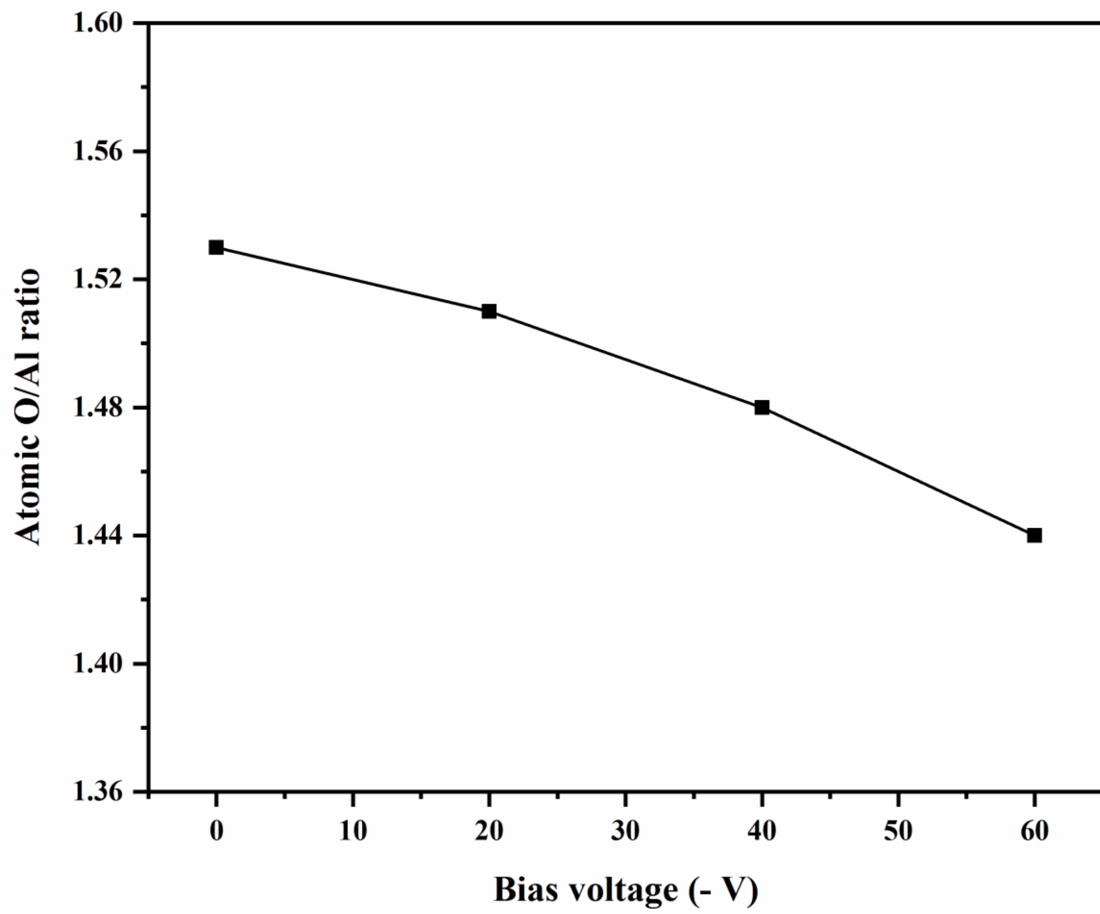

Fig. 7. Atomic O/Al ratios of as-deposited Al_2O_3 thin films deposited on Si substrate at various bias voltages.

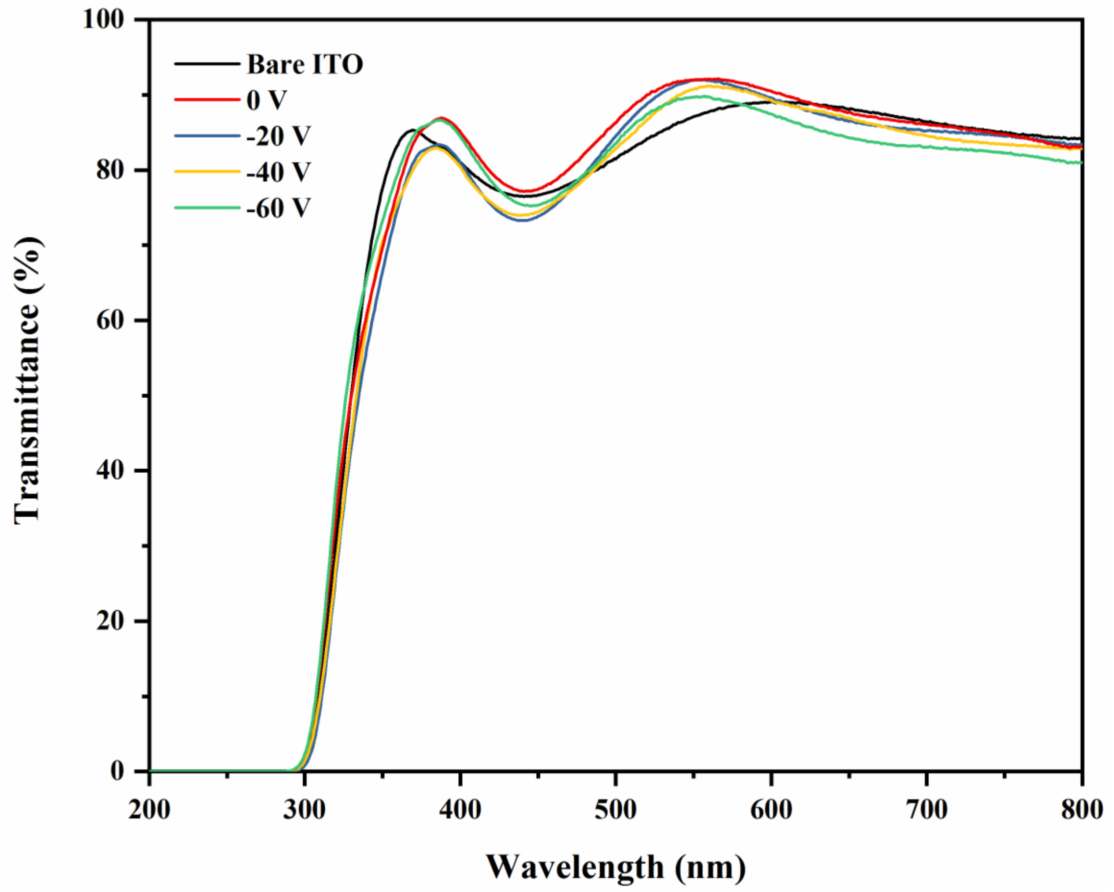

Fig. 8. Transmittance spectra of Al_2O_3 thin films deposited on ITO substrate at various bias voltages.